International Journal of Thermophysics, Vol. 25, No. 6, November 2004 (© 2004)

A Rigorous Thermodynamic Property Model for Fluid-Phase 1,1-Difluoroethane (R-152a)

I M. Astina[1] **and H. Sato**[2,3]

Received June 7, 2004

A new thermodynamic property model for the Helmholtz free energy with rational third virial coefficients for fluid-phase 1,1-difluoroethane (R-152a) was developed. The model was validated by existing experimental data for temperatures from the triple point to 450 K and pressures up to 60 MPa. Reasonable behavior of the second and third virial coefficients was confirmed from intermolecular potential models. The estimated uncertainties are 0.1% in density for the gaseous and liquid phases, 0.4% in density for the supercritical region, 0.05% in speed of sound for the gaseous phase, 2% in speed of sound for the liquid phase, and 1% in specific heat capacities for the liquid phase. From the reasonable behavior of the ideal curves and the third virial coefficients, the model can be assumed reliable in representing the thermodynamic properties not only at states with available experimental data but also at states for which no experimental data are available.

KEY WORDS: 1,1-difluoroethane; Helmholtz energy equation of state; HFC refrigerant; intermolecular potential; R-152a; thermodynamic model; virial coefficients.

1. INTRODUCTION

1,1-Difluoroethane (R-152a) is a hydrofluorocarbon (HFC) refrigerant that shows theoretically high performance in applications for heat pumps. Several efforts to use R-152a as an alternative refrigerant were made in the 1990s. Investigations of both experiments and modeling for the thermodynamic properties of R-152a are still ongoing. Several thermodynamic

[1]Department of Mechanical Engineering, Institut Teknologi Bandung, Jalan Ganesha 10, Bandung 40132, Indonesia.
[2]Department of System Design Engineering, Keio University, 3-14-1 Hiyoshi, Kohoku-ku, Yokohama 223-8522, Japan.
[3]To whom correspondence should be addressed. E-mail: hsato@sd.keio.ac.jp

0195-928X/04/1100-1713/0

property models for the fluid-phase of R-152a have been proposed such as the Helmholtz energy equation of state [1, 2], the MBWR equation of state [3], and the virial equation of state [4].

Detailed aspects for developing a new model with a theoretical background were given in a previous paper on R-32 [5]. Models for R-125 and R-134a were developed by means of the same procedure [6, 7]. This paper presents development of a thermodynamic property model, using this same concept for the fluid-phase of R-152a in a series of studies on thermodynamic modeling of HFC refrigerants.

2. MAIN PARAMETERS AND ANCILLARY EQUATIONS

Physical parameters and ancillary equations are needed for the development and implementation of the thermodynamic property model. The critical parameters used are the critical temperature of 386.41 K [8], the critical density of 368 $kg \cdot m^{-3}$ [8], and the critical pressure of 4.516 MPa derived from the extrapolation of the vapor-pressure equation developed in this work. Other parameters are the triple-point temperature of 154.56 K [10], the gas constant of 8.314472 $J \cdot mol^{-1} \cdot K^{-1}$ [11], and the molar mass of 0.066050 $kg \cdot mol^{-1}$.

Three ancillary equations for the vapor pressure and saturated-vapor and saturated-liquid densities from the triple point to the critical point were developed in this work. The vapor-pressure equation can be written as

$$\ln \frac{p_s}{p_c} = \frac{T_c}{T} \sum_{i=1}^{4} N_i \left(1 - \frac{T}{T_c}\right)^{t_i}, \tag{1}$$

where $N_1 = -7.347239$, $t_1 = 1$, $N_2 = 1.519178$, $t_2 = 1.5$, $N_3 = -1.892860$, $t_3 = 2.5$, $N_4 = -3.029767$, and $t_4 = 5$. The saturated-liquid density equation can be expressed as

$$\frac{\rho'}{\rho_c} - 1 = \sum_{i=1}^{4} N_i \left(1 - \frac{T}{T_c}\right)^{t_i}, \tag{2}$$

where $N_1 = 1.842790$, $t_1 = 1/3$, $N_2 = 0.7160983$, $t_2 = 2/3$, $N_3 = 0.2037560$, $t_3 = 1$, $N_4 = 0.2454605$, and $t_4 = 3$. The saturated-vapor density equation can be expressed as

$$\ln \frac{\rho''}{\rho_c} = \sum_{i=1}^{5} N_i \left(1 - \frac{T}{T_c}\right)^{t_i}, \tag{3}$$

where $N_1 = -2.117459$, $t_1 = 1/3$, $N_2 = -6.430882$, $t_2 = 1$, $N_3 = -19.21177$, $t_3 = 3$, $N_4 = -66.492476$, $t_4 = 7$, $N_5 = 5.603786$, and $t_5 = 10$.

3. DEVELOPMENT OF THERMODYNAMIC PROPERTY MODEL

Input data for thermodynamic modeling include experimental measurements of *PVT* and caloric properties. The distribution of the selected data for R-152a is shown in Fig. 1. The available reliable experimental data at low temperature are scarce. *PVT* data for the liquid phase consist of 26 points of Geller et al. [12], 126 points of Magee [10], and 289 points from Tillner-Roth and Baehr [13]. *PVT* data in the superheated-vapor phase consist of 20 points of Dressner and Bier [14], 319 points of Tillner-Roth and Baehr [15], and 28 points of Tillner-Roth and Baehr [13]. *PVT* data in the supercritical region consist of 27 points of Blanke and Weiss [16], 8 points of Dressner and Bier [14], 8 points of Magee [10], 44 points of Tillner-Roth and Baehr [15], and 88 points of Tillner-Roth and Baehr [13].

Experimental caloric data consist of the isochoric specific heat capacity and the speed of sound. Eighty-five points for the isochoric specific heat capacity in the liquid phase from Magee [17] are available, including 66 points of derived data for the saturated-liquid specific heat capacity. Speed-of-sound data in the gaseous phase were selected from 44 points of Hozumi et al. [18] and 148 points of Gillis [19], and the data for the liquid phase consist of 51 points of Beliajeva et al. [20] and 50 points from Grebenkov et al. [21].

There are no isochoric specific heat capacity measurements in the gaseous phase. This property is directly related to the second derivatives of the Helmholtz free energy with respect to temperature. The final equation of state was greatly improved by including measurements in the fit for both the liquid and gaseous phases. By using an accurate virial equation

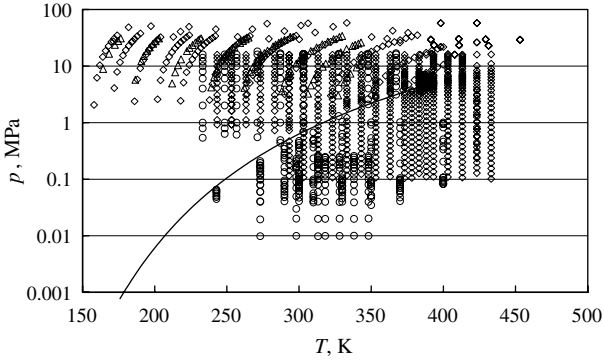

Fig. 1. Selected experimental data for developing the new thermodynamic property model. (◊) *PVT*; (Δ) c_v; (○) *w*.

of state [9] and the ideal-gas isobaric specific heat capacity equation, the isochoric specific heat capacities were calculated in the gaseous phase at pressures lower than 2 MPa. The second and third virial coefficients were also included in modeling. These data were calculated from the virial coefficient relation given in Ref. 9.

Two critical constraints were included in fitting by setting the first and second derivatives of pressure with respect to density at the critical point to zero. The Maxwell criterion has an important role in modeling the saturation states. This criterion (equal pressures and Gibbs energies at the saturation temperature) requires the vapor pressure and the saturated-liquid and saturated-vapor densities at a given temperature. Since data satisfying these requirements are not available, the three ancillary equations presented earlier were used to calculate saturation properties and were used in fitting to describe the vapor pressure and the saturated-vapor and saturated-liquid densities from the triple point to the critical point.

4. NEW THERMODYNAMIC PROPERTY MODEL

The new thermodynamic property model consists of an ideal-gas part and a residual part. The ideal-gas part provides the properties of the fluid in the ideal-gas state. The residual part provides the properties of the real fluid (the residual separated from the contribution of the ideal gas). The relations among the thermodynamic properties are given in Table I. All of these properties can be calculated from the model.

The ideal-gas part was derived by means of integration of the ideal-gas isobaric specific heat capacity equation. This equation was established by fitting to theoretical values derived by Yokozeki et al. [22], and optimized by introducing polynomial and Planck–Einstein terms. The terms were selected in accordance with an original genetic optimization method, which will be introduced in another paper. The integral boundary condition was defined with a reference state of $200\,\mathrm{kJ\cdot kg^{-1}}$ for enthalpy and $1\,\mathrm{kJ\cdot kg^{-1}\cdot K^{-1}}$ for entropy for the saturated liquid state at 273.15 K. The ideal-gas part is written as

$$\alpha^{\mathrm{o}}(\delta,\tau) = \ln\left(\frac{\delta}{\tau}\right) + N_0^{\mathrm{o}} + N_1^{\mathrm{o}}\tau + N_2^{\mathrm{o}}\tau^{-0.5} + N_3^{\mathrm{o}}\tau^{0.25} + \sum_{i=4}^{5} N_i^{\mathrm{o}} \ln\left\{1 - \exp\left(-b_i^{\mathrm{o}}\tau\right)\right\}, \tag{4}$$

where $N_0^{\mathrm{o}} = -9.508135074$, $N_1^{\mathrm{o}} = 6.812068779$, $N_2^{\mathrm{o}} = -7.285916044$, $N_3^{\mathrm{o}} = 6.741130104$, $N_4^{\mathrm{o}} = 1.978152028$, $N_5^{\mathrm{o}} = 5.880826311$, $b_4^{\mathrm{o}} = 1.753741145$, and

Table I. Relations of Thermodynamic Properties from Helmholtz Free Energy

Property	Relations
Compressibility factor	$Z = 1 + \delta\alpha_\delta^r$
Pressure	$p(\delta,\tau)/(\rho RT) = 1 + \delta\alpha_\delta^r$
Fugacity	$f(\delta,\tau) = p\exp\{\alpha^r + \delta\alpha_\delta^r - \ln(1+\delta\alpha_\delta^r)\}$
cellSpecific heat capacity of ideal gas	$c_p^o(\tau)/R = 1 - \tau^2\alpha_{\tau\tau}^o = 1 + c_v^o(\tau)/R$
Isobaric specific heat capacity	$c_p(\delta,\tau)/R = c_v(\delta,\tau)/R + \frac{(1+\delta\alpha_\delta^r - \delta\tau\alpha_{\delta\tau}^r)^2}{(1+2\delta\alpha_\delta^r + \delta^2\alpha_{\delta\delta}^r)}$
Isochoric specific heat capacity	$c_v(\delta,\tau)/R = -\tau^2(\alpha_{\tau\tau}^o + \alpha_{\tau\tau}^r)$
Saturated-liquid specific heat capacity	$c_s'(\delta',\tau)/R = \frac{c_v(\delta',\tau)}{R} + \frac{(1+\delta'\alpha_\delta^{r'} - \delta'\tau\alpha_{\delta\tau}^{r'})}{(1+2\delta'\alpha_\delta^{r'} + \delta'^2\alpha_{\delta\delta}^{r'})} \times \left\{1 + \delta'\alpha_\delta^{r'} - \delta'\tau\alpha_{\delta\tau}^{r'} - \frac{1}{R\rho_c\delta'}\frac{dp(\delta',\tau)}{dT}\right\}$
Isothermal compressibility	$\kappa(\delta,\tau)\rho RT = \{1 + 2\delta\alpha_\delta^r + \delta^2\alpha_{\delta\delta}^r\}^{-1}$
Isobaric expansion coefficient	$\beta(\delta,\tau)\cdot T = (1+\delta\alpha_\delta^r - \tau\delta\alpha_{\delta\tau}^r)(1 + 2\delta\alpha_\delta^r + \delta^2\alpha_{\delta\delta}^r)$
Joule–Thomson coefficient	$\mu(\delta,\tau)R\rho = \frac{-(\delta\alpha_\delta^r + \delta^2\alpha_{\delta\delta}^r + \delta\tau\alpha_{\delta\tau}^r)}{(1+\delta\alpha_\delta^r - \delta\tau\alpha_{\delta\tau}^r)^2 + c_v(\delta,\tau)/R(1+2\delta\alpha_\delta^r + \delta^2\alpha_{\delta\delta}^r)}$
Specific enthalpy	$h(\delta,\tau)/(RT) = \tau(\alpha_\tau^o + \alpha_\tau^r) + 1 + \delta\alpha_\delta^r$
Specific entropy	$s(\delta,\tau)/R = \tau(\alpha_\tau^o + \alpha_\tau^r) - (\alpha^o + \alpha^r)$
Specific Gibbs free energy	$g(\delta,\tau)/(RT) = 1 + \alpha^o + \alpha^r + \delta\alpha_\delta^r$
Specific internal energy	$u(\delta,\tau)/(RT) = \tau(\alpha_\tau^o + \alpha_\tau^r)$
Speed of sound	$w^2(\delta,\tau)/(RT) = 1 + 2\delta\alpha_\delta^r + \delta^2\alpha_{\delta\delta}^r + \frac{(1+\delta\alpha_\delta^r - \delta\tau\alpha_{\delta\tau}^r)^2}{c_v(\delta,\tau)/R}$
Second virial coefficient	$B(\tau)\rho_c = \lim_{\delta\to 0}\alpha_\delta^r$
Third virial coefficient	$C(\tau)\rho_c^2 = \lim_{\delta\to 0}\alpha_{\delta\delta}^r$

Abbreviations: $\alpha_\delta = (\frac{\partial\alpha}{\partial\delta})_\tau$, $\alpha_\tau = (\frac{\partial\alpha}{\partial\tau})_\delta$, $\alpha_{\delta\delta} = (\frac{\partial^2\alpha}{\partial\delta^2})_\tau$, $\alpha_{\tau\tau} = (\frac{\partial^2\alpha}{\partial\tau^2})_\delta$, $\alpha_{\delta\tau} = (\frac{\partial^2\alpha}{\partial\delta\partial\tau})$, $\delta = \frac{\rho}{\rho_c}$, $\tau = \frac{T_c}{T}$

$b_5^o = 4.360150337$. The residual part was determined from a multi-property regression and genetic optimization for selecting terms in the equation. The residual part is written as

$$\alpha^r = \sum_{i=1}^{8} N_i\delta^{d_i}\tau^{t_i} + \sum_{i=9}^{11} N_i\delta^{d_i}\tau^{t_i}\exp(-\delta) + \sum_{i=12}^{14} N_i\delta^{d_i}\tau^{t_i}\exp(-\delta^2) + \sum_{i=15}^{17} N_i\delta^{d_i}\tau^{t_i}\exp(-\delta^3), \quad (5)$$

Table II. Numerical Coefficients and Parameters of the Residual Part

i	N_i	d_i	t_i
1	$1.753847317 \times 10^{0}$	1	0.5
2	$-4.049760759 \times 10^{0}$	1	1.125
3	$-2.277389257 \times 10^{-1}$	1	2.875
4	$7.087751950 \times 10^{-1}$	2	0.875
5	$-5.528619502 \times 10^{-1}$	2	1.875
6	$-3.025046686 \times 10^{-2}$	3	0.5
7	$1.396289974 \times 10^{-1}$	3	1.875
8	$1.121238954 \times 10^{-4}$	4	4
9	$1.181005890 \times 10^{0}$	1	1.25
10	$1.535785579 \times 10^{0}$	2	2
11	$7.468363045 \times 10^{-1}$	3	2.75
12	$-1.252266405 \times 10^{-1}$	1	6
13	$-3.898223986 \times 10^{-2}$	2	9
14	$-7.260588801 \times 10^{-2}$	3	6
15	$-2.659302250 \times 10^{-3}$	3	22
16	$4.210849329 \times 10^{-3}$	4	20
17	$2.015953966 \times 10^{-4}$	5	32
$R = 8.314472\,\mathrm{J \cdot mol^{-1} \cdot K^{-1}}$		ρ_c=368 kg·m^{-3}	
$T_c = 386.41\,\mathrm{K}$		$p_c = 4.5160\,\mathrm{MPa}$	

where the numerical coefficients and parameters are given in Table II. The reducing parameters for these equations are $\delta = \rho/\rho_c$ and $\tau = T_c/T$. The calculated thermodynamic properties from the new model, which are very useful to verify computer program, are given in Table III.

5. ASSESSMENT

Representation of thermodynamic properties from the new model was assessed by comparing with experimental data. Deviations of the thermodynamic properties were calculated with the new model as the baseline. Table IV shows the statistical results for the accuracy of the thermodynamic properties at saturation and in the single phase.

The ideal-gas isobaric specific heat capacities of Yokozeki et al. [22] are reproduced from 120 to 1000 K within 0.05% as shown in Fig. 2. The equations of Outcalt and McLinden [3] and Tillner-Roth [1] show systematically higher deviations from the Yokozeki et al. data.

The representation of the saturation properties can be assessed by comparing values calculated from the new model with measurements of

Table III. Calculated Thermodynamic Properties of R-152a for Verifying Computer Program

p (MPa)	T (K)	ρ(kg·m^{-3})	c_v (kJ·kg^{-1}·K^{-1})	c_p (kJ·kg^{-1}·K^{-1})	w (m·s^{-1})	h (kJ·kg^{-1})	s (kJ·kg^{-1}·K^{-1})
Single phase							
0.01	200	1108.30	1.02563	1.53226	1144.46	83.0731	0.504046
0.1	250	3.32533	0.85146	1.02093	185.395	490.101	2.17402
0.5	300	14.9178	1.01270	1.25049	190.307	528.281	2.12554
1	250	1011.40	1.06828	1.61778	887.901	162.066	0.852079
2	450	39.2134	1.27176	1.47906	230.750	703.818	2.44002
3	450	62.4333	1.29309	1.56254	221.167	692.526	2.37021
5	300	910.768	1.14104	1.75988	681.439	247.753	1.14904
15	350	829.854	1.22465	1.86556	577.309	339.639	1.39677
25	400	764.468	1.30865	1.92116	526.849	433.427	1.61365
40	250	1069.55	1.10283	1.54070	1076.73	183.511	0.78821
45	300	999.404	1.17500	1.61174	920.812	265.090	1.06788
50	450	782.051	1.40653	1.86403	612.067	528.382	1.76108
Saturation[a]							
0.00608	200	1108.30	1.02563	1.53227	1144.44	83.0708	0.504052
		0.243503	0.688696	0.822899	172.126	452.530	2.35135
0.62958	300	895.050	1.14163	1.80605	635.933	246.936	1.16245
		19.5363	1.05165	1.34292	184.955	523.189	2.08329
0.01	206.996	1095.05	1.02888	1.54024	1106.00	93.8198	0.556861
		0.387819	0.709506	0.846608	174.478	457.773	2.31513
2	345.817	755.354	1.23824	2.22690	400.169	336.806	1.43550
		67.2945	1.25774	1.99694	166.520	542.188	2.02940

[a]The upper line is for saturated liquid and the second line is for saturated vapor.

Table IV. Deviations of Measurements from the New Thermodynamic Property Model for R-152a[a]

Reference	Y	N	P(MPa)	T(K)	Phase	AAD (%)	BIAS(%)	STD (%)	Max (%)	N_{out}
Baehr and Tillner-Roth [29]	p_s	55	–	301–386	–	0.18	0.18	0.030	0.23	–
Blanke and Weiss [16]	p_s	36	–	155–260	–	0.082	0.0074	0.15	0.83	5
Duarte-Garza and Magee [30]	p_s	21	–	155–250	–	0.092	0.0019	0.13	0.30	–
Fransson et al. [31]	p_s	5	–	303–385	–	0.67	0.67	0.28	0.89	–
Higashi et al. [8]	p_s	44	–	273–386	–	0.059	0.037	0.057	0.17	–
Holcomb et al. [23]	p_s	33	–	312–383	–	0.18	0.17	0.20	0.10	–
Kamei et al. [25]	p_s	24	–	250–365	–	0.069	0.044	0.10	0.41	–
McLinden [26]	p_s	21	–	273–373	–	0.051	0.019	0.054	0.083	–
Mears et al. [27]	p_s	27	–	204–377	–	2.1	1.7	3.0	9.7	7
Sato et al. [32]	p_s	41	–	273–373	–	0.047	0.018	0.047	0.074	–
Silva and Weber [33]	p_s	38	–	220–273	–	0.097	−0.097	0.026	0.14	1
Tillner-Roth [34]	p_s	40	–	155–232	–	0.24	0.22	0.36	1.2	6
Yada et al. [35]	p_s	13	–	305–385	–	0.13	0.11	0.17	0.53	–
Zhao et al. [36]	p_s	167	–	237–368	–	0.20	−0.092	0.24	0.75	1
Blanke and Weiss [16]	ρ'	19	–	160–308	–	0.061	−0.061	0.029	0.12	–
Geller et al. [12]	ρ'	19	–	160–340	–	0.11	0.0050	0.13	0.22	–
Higashi et al. [8]	ρ'	10	–	371–386	–	0.35	0.047	0.46	0.90	3
Holcomb et al. [23]	ρ'	33	–	312–384	–	0.15	−0.15	0.077	0.27	–
Kabata et al.[24]	ρ'	10	–	371–386	–	0.35	0.047	0.46	0.90	3
Kamei et al. [25]	ρ'	24	–	250–365	–	0.14	−0.12	0.13	0.29	–
Magee [10]	ρ'	9	–	157–318	–	0.027	0.026	0.032	0.095	–
McLinden [26]	ρ'	29	–	233–373	–	0.15	−0.15	0.11	0.34	–
Mears et al. [27]	ρ'	11	–	232–353	–	0.27	−0.22	0.26	0.77	–
Wang et al. [28]	ρ'	11	–	376–386	–	1.1	−0.77	1.4	2.9	4
Higashi et al. [8]	ρ''	11	–	374–386	–	1.0	0.40	1.6	2	2
Holcomb et al. [23]	ρ''	33	–	312–384	–	1.0	1.0	0.75	2.8	1
Kabata et al. [24]	ρ''	11	–	374–386	–	1.0	0.40	1.2	1.9	2

Kamei et al. [25]	ρ''	24	–	250–364	–	0.50	−0.50	0.55	1.0	–
Wang et al. [28]	ρ''	11	–	377–386	–	1.1	0.16	1.4	1.9	3
Magee [10]	c'_s	66	–	163–315	–	0.58	0.58	0.27	1.0	–
Gunther and Steimle [42]	c'_p	8	–	203–323	–	0.42	−0.065	0.55	1.1	–
Beliajeva et al. [20]	w'	17	–	250–330	–	0.4	0.17	0.42	0.8	–
Blanke and Weiss [16]	ρ	209	0.59–31	160–453	L	0.073	−0.059	0.074	0.72	1
Defibaugh and Moldover [37]	ρ	1011	0.70–6.5	243–371	L	0.035	−0.028	0.025	0.061	–
Dressner and Bier [14]	ρ	150	0.23–58	333–423	G	0.11	−0.035	0.20	0.92	2
Geller et al. [12]	ρ	97	0.65–58	159–470	L	0.14	−0.069	0.17	0.57	2
Iso and Uematsu [38]	ρ	241	1.25–10	313–400	L	0.74	0.40	1.1	3.9	12
Magee [10]	ρ	134	2.05–35	158–400	L	0.045	−0.002	0.061	0.16	–
Mears et al. [27]	ρ	22	1.81–4.6	345–397	G	1.3	−1.0	0.96	0.94	6
Strom and Gren [39]	ρ	21	0.47–1.6	261–323	L	0.82	0.70	0.59	1.3	–
Tillner-Roth and Baehr [15]	ρ	335	0.10–16	293–433	G	0.068	0.005	0.19	1.7	2
Tillner-Roth and Baehr [13]	ρ	413	0.73–16	243–413	L	0.14	−0.029	0.30	1.9	4
Yada et al. [35]	ρ	16	4.2–8.8	383–423	G	12	12	7.8	30	–
Zhao et al. [36]	ρ	257	0.09–6.1	253–404	G	1.1	−0.64	1.3	5.0	82
Kubota [43]	c_p	20	0.50–1.4	313–354	L	4.6	4.6	1.4	7.4	–
Nakagawa et al. [44]	c_p	70	1.0–3.2	210–360	L	1.2	−1.2	0.20	1.6	1
Porichanski et al. [45]	c_p	304	2.0–20	181–424	L	1.2	0.38	1.6	6.6	27
Sato and Watanabe [46]	c_p	36	1.0–3.2	276–360	L	1.2	−1.2	0.21	1.6	–
Magee [10]	c_v	85	3.0–34	163–342	L	0.48	0.44	0.35	1.2	–
Beliajeva et al. [40]	w	52	0.54–18	233–303	L	1.2	1.2	0.34	2.0	1
Gillis [19]	w	148	0.03–1.0	243–400	G	0.016	0.01	0.021	0.082	
Grebenkov et al. [21]	w	54	0.44–17	287–367	L	0.56	0.28	0.59	1.4	2
He et al. [41]	w	24	0.20–0.42	294–323	G	0.63	0.63	0.20	1.0	1
Hozumi et al. [18]	w	92	0.19–0.22	273–348	G	0.014	−0.014	0.0091	0.071	2

[a] $\mathrm{AAD} = \sum_{i=1}^{n} |\Delta_i|/n$; $\mathrm{STD} = \sqrt{\sum_{i=1}^{n} (\Delta_i - \mathrm{BIAS})^2/(n-1)}$; $\mathrm{BIAS} = \sum_{i=1}^{n} \Delta_i/n$; N is the number of data points included in the evaluation; $\Delta = 100(Y - Y_{\mathrm{cal}})/Y_{\mathrm{cal}}$ where Y is an evaluated property.

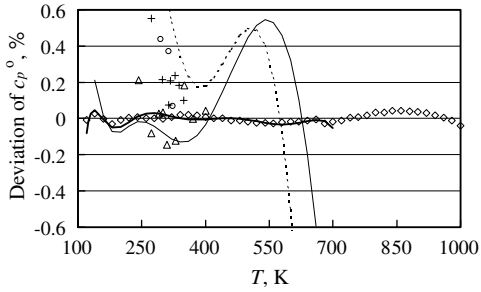

Fig. 2. Deviations of ideal-gas isobaric specific heat capacities from the new thermodynamic property model. (Δ) Gillis [19]; (○) He et al. [41]; (+) Hozumi et al. [18]; (◇) Yokozeki et al. [22]; (- - -) Tillner-Roth [1]; (—) Outcalt and McLinden [3]; (———) Sato et al. [48].

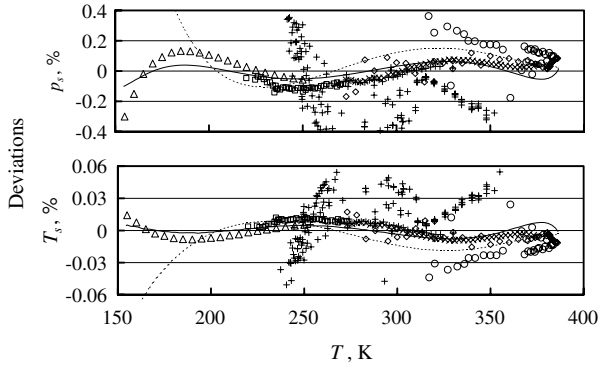

Fig. 3. Deviations of vapor pressures and saturation temperatures from the new thermodynamic property model. (Δ) Duarte-Garza and Magee [30]; (◇) Higashi et al. [8]; (○) Holcomb et al. [23]; (×) Sato et al. [32]; (□) Silva and Weber [33]; (+) Zhao et al. [36]; (- - -) Tillner-Roth [1]; (——) Outcalt and McLinden [3].

the vapor pressure and the saturated-liquid and saturated-vapor densities. Comparisons to the other models were also assessed. The deviations of vapor pressures and saturation temperatures are shown in Fig. 3. Deviations for the saturated-liquid and saturated-vapor densities are given in Fig. 4. Both the new model and also the older ones show larger discrepancies in density for the states near the critical point. The uncertainties are 0.1% for the vapor pressure, 0.05% for the saturation temperatures, 0.2%

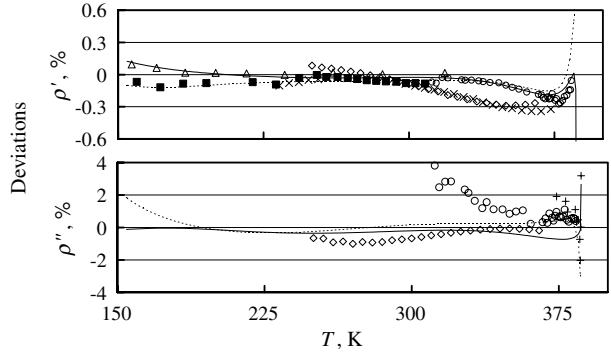

Fig. 4. Deviations of saturated-liquid and saturated-vapor densities from the new thermodynamic property model. (△) Wang et al. [28]; (○) Holcomb et al. [23]; (■) Blanke and Weiss [16]; (+) Higashi et al. [8]; (×) McLinden [26]; (- - - - -) Tillner-Roth [1]; (——) Outcalt and McLinden [3].

for the saturated-liquid densities, and 0.5% for the saturated-vapor densities. Available experimental data for the saturated-vapor densities are very scarce at lower temperatures. Calculated values from the new model for the saturated-liquid densities fall between the data of Wang et al. [28] and of Blanke and Weiss [16].

Density deviations over a wide range of single-phase gaseous and liquid states are shown in Fig. 5 for high temperatures and Fig. 6 for low temperatures. The density deviation for the superheated-vapor phase is represented within 0.1%, that for the liquid phase is within 0.1%, and that for the supercritical region is within 0.4%.

The speed of sound in the gaseous phase is reproduced with an uncertainty of 0.02%, while the speed of sound in the liquid phase is represented within 1%. These results are shown in Fig. 7. The isobaric and isochoric specific heat capacities in the liquid phase are shown in Fig. 8. The uncertainty for the isobaric specific heat capacity is 2%, and that for the isochoric specific heat capacity is 1%. The saturated-liquid specific heat capacity data of Magee [17] is reproduced with an uncertainty of 1% as shown in Fig. 9.

Critical parameters were determined from the new model. The calculated critical temperature and density are 367.9987 $kg \cdot m^{-3}$ and 386.4101 K. Using these values, the critical pressure calculated from the new model is 4.5160 MPa. This demonstrates that the fitting of the critical constraints in the regression adequately yielded the critical parameters.

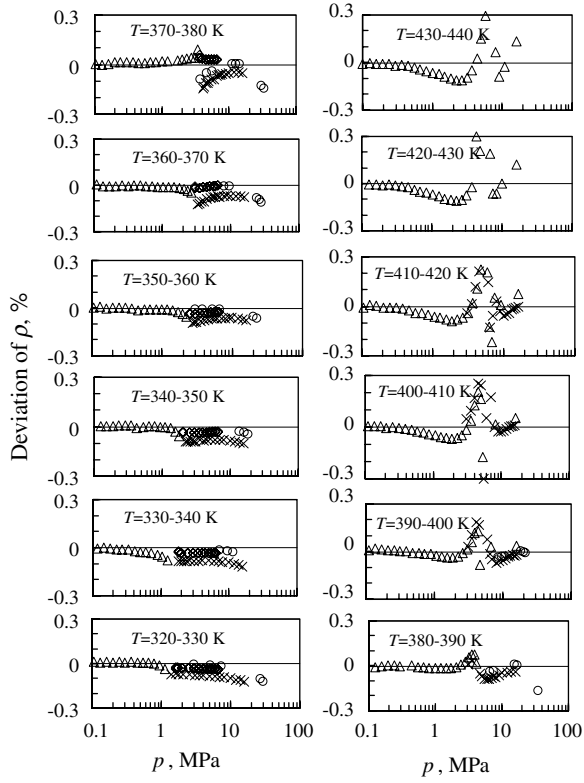

Fig. 5. Deviations of the density at temperatures higher than 320 K from the new thermodynamic property model. (□) Blanke and Weiss [16]; (◊) Defibaugh and Moldover [37]; (○) Magee [17]; (△) Tillner-Roth and Baehr [15]; (×) Tillner-Roth and Baehr [13].

6. EXTRAPOLATION BEHAVIOR AND FEATURES

In general, the most accurate model will give reasonable second virial coefficients that agree with intermolecular potential theory. However, third virial coefficients derived from existing models do not agree well with intermolecular potential models. Figure 10 shows large discrepancies of the third virial coefficients derived from several models. Yokozeki et al. [22] calculated the second and third virial coefficients from the Stockmayer intermolecular potential model. The behavior of several models at extreme temperatures is also shown. Both the second and third virial coefficients at extreme temperatures derived from the new model are asymptotically close

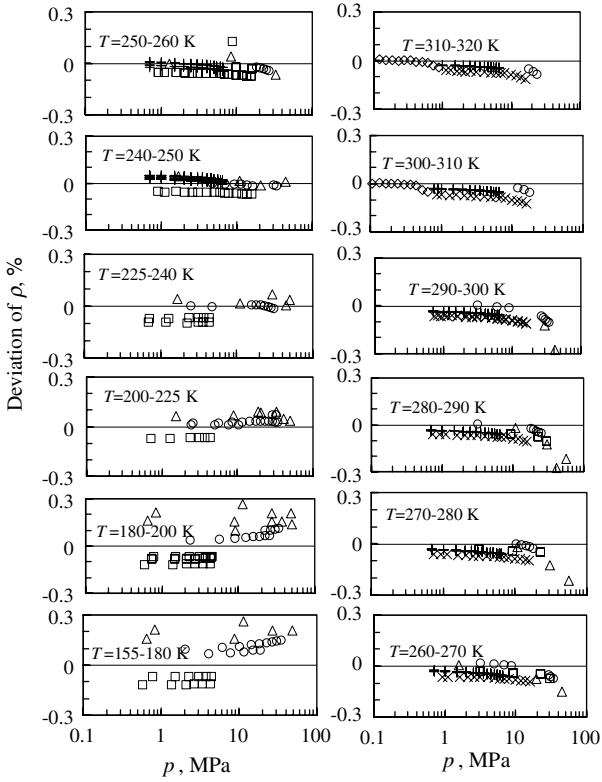

Fig. 6. Deviations of the density at temperatures lower than 320 K from the new thermodynamic property model. (□) Blanke and Weiss [16]; (+) Defibaugh and Moldover [37]; (Δ) Geller et al. [12]; (○) Magee [17]; (×) Tillner-Roth and Baehr [13].

to those calculated by Yokozeki et al. [22] from the Stockmayer intermolecular potential model and as close to those from Span and Wagner [2].

Specific heat capacities in the gaseous phase are useful in ascertaining the quality of a model. Figure 11 compares the isochoric specific heat capacities calculated from several models. Large discrepancies are shown in the gaseous phase near saturation. Additionally, making experimental measurements for verification of a model is difficult due to shortcomings in the experiments.

Extrapolations of the thermodynamic properties from the new model are given in Figs. 12–15. Although the amount of available data for these properties is scarce, the values of c_v in Fig. 12, c_p in Fig. 13, w in Fig. 14,

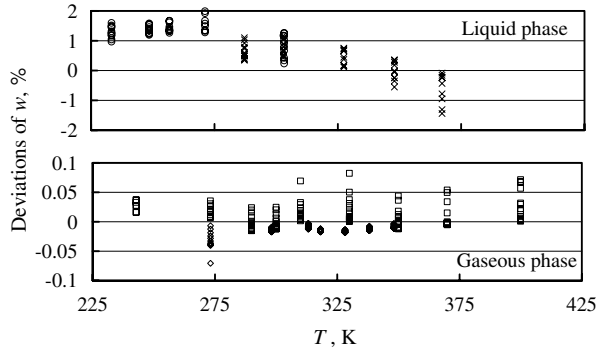

Fig. 7. Deviations of speed of sound from the new thermodynamic property model. (×) Grebenkov et al. [21]; (□) Gillis [19]; (○) Beliajeva et al. [20]; (◇) Hozumi et al. [18].

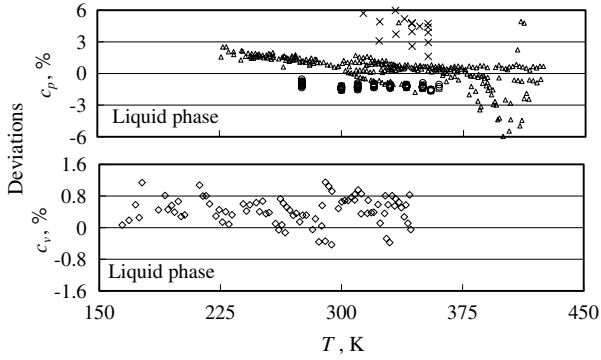

Fig. 8. Deviations of specific heat capacities in the liquid phase from the new thermodynamic property model. (◇) Magee [10]; (×) Kubota [43]; (○) Nakagawa et al. [44]; (Δ) Porichanski et al. [45]; (□) Sato and Watanabe [46].

and *PVT* in Fig. 15 confirm that the new model satisfactorily represents the thermodynamic values over the wide entire fluid phase.

Reasonable ideal curves can be derived from the new model as shown in Fig. 16. The new model shows a qualitatively reasonable representation from a physical viewpoint at extremely high temperatures and pressures, even in regions where no experimental data are available.

Based on this result, the new model should be able to represent the thermodynamic properties of the entire fluid phase for pressures up to 350 MPa and temperatures up to the limits of dissociation. A pressure–enthalpy diagram from the new model is provided in Fig. 17.

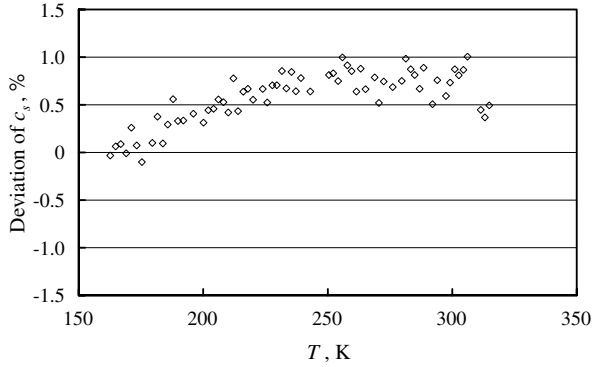

Fig. 9. Deviations of saturated-liquid specific heat capacity from the new thermodynamic property model. (◇) Magee [10].

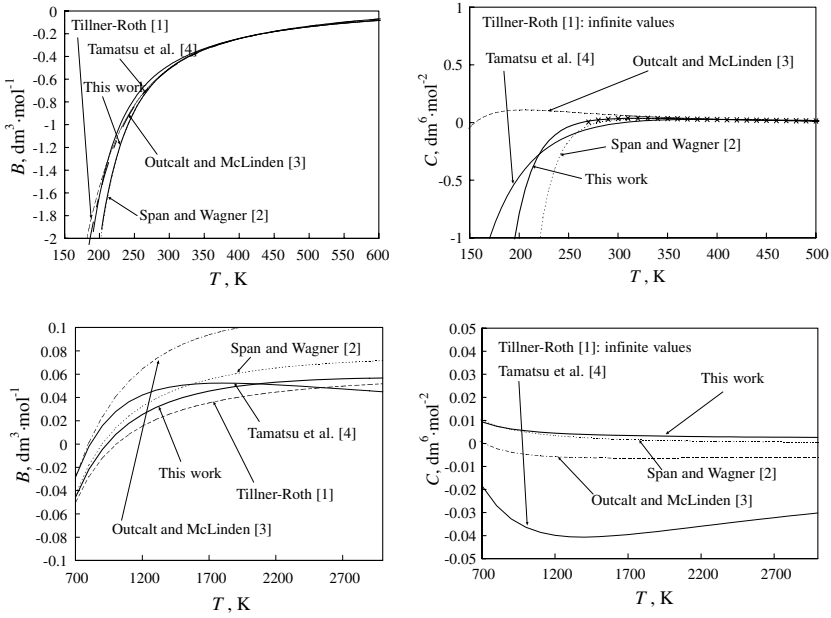

Fig. 10. Second and third virial coefficients from several fluid-phase thermodynamic property models. (×) Yokozeki et al. [22].

7. CONCLUSION

A thermodynamic property model for fluid-phase R-152a was established with rational second and third virial coefficients. The new model

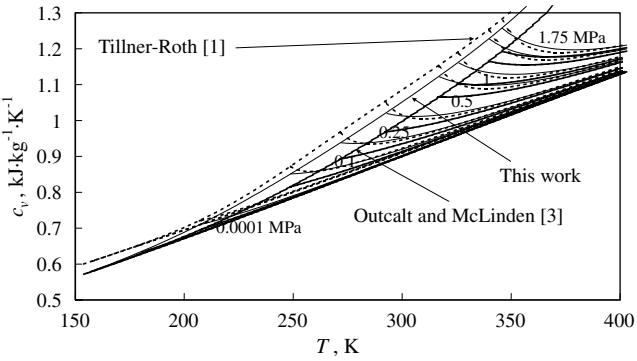

Fig. 11. Isochoric specific heat capacity in the gaseous phase from several fluid-phase thermodynamic property models.

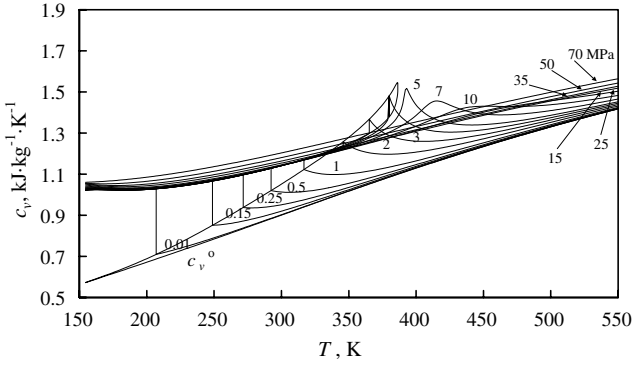

Fig. 12. Isobaric lines of isochoric specific heat capacity from the new thermodynamic property model.

provides reliable thermodynamic properties even at very low temperatures and near saturation in the gaseous phase. The specific heat capacity values in the gaseous phase near saturation are reasonably represented without any thermodynamic inconsistencies.

The new model is valid in the fluid phase for temperatures from the triple point to 450 K and pressures up to 60 MPa. The second and third virial coefficients are in agreement with those derived in accordance with the intermolecular potential theory. The estimated uncertainties are 0.1% in density for the gaseous phase, 0.1% in density for the liquid phase, 0.4%

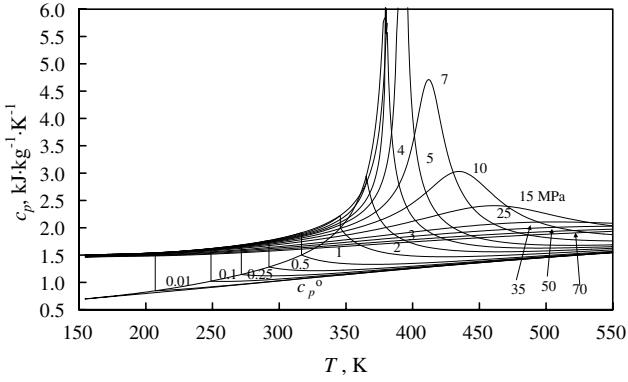

Fig. 13. Isobaric lines of isobaric specific heat capacity from the new thermodynamic property model.

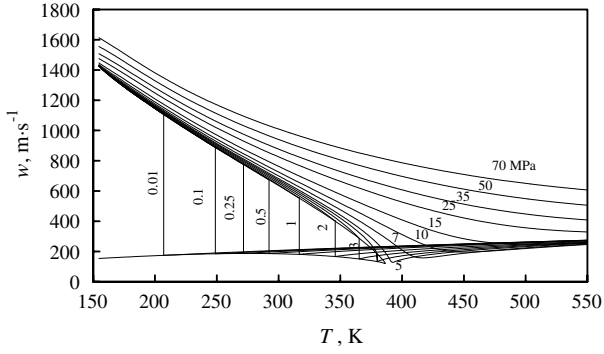

Fig. 14. Isobaric lines of speed of sound from the new thermodynamic property model.

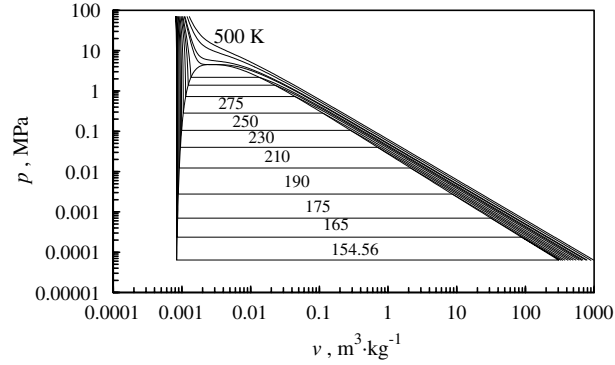

Fig. 15. *PVT* diagram from the new thermodynamic property model.

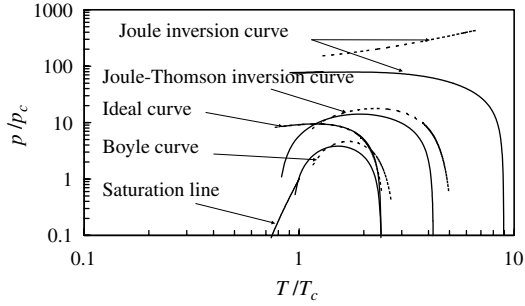

Fig. 16. Comparison of ideal curves. (—) the new thermodynamic property model. (----) Tillner-Roth [1].

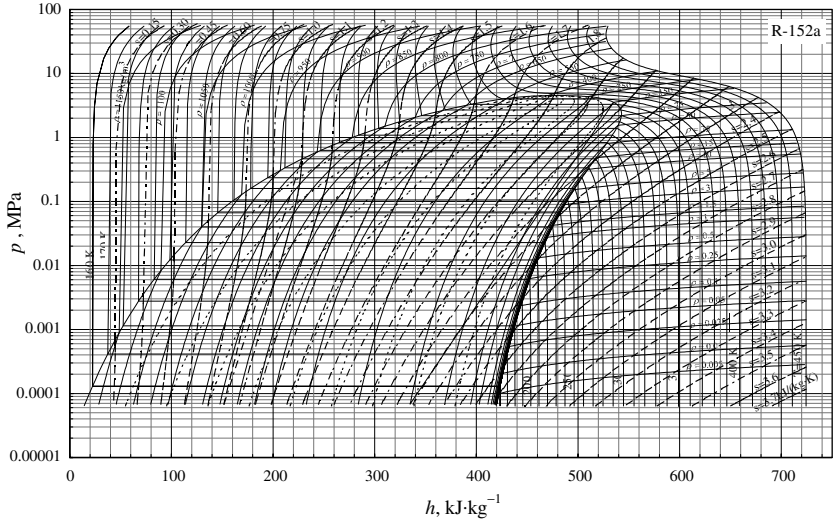

Fig. 17. Pressure–enthalpy diagram for R-152a calculated from the new thermodynamic property model.

in density for the supercritical region, 0.05% in speed of sound for the gaseous phase, 2% in speed of sound for the liquid phase, and 1% in isochoric specific heat capacity for the liquid phase.

ACKNOWLEDGMENT

The authors would like to thank Dr. Eric W. Lemmon, NIST, for his kind and strict comments and valuable suggestions.

NOMENCLATURE

a	specific Helmholtz free energy
α	reduced Helmholtz free energy, $\alpha = \alpha^{o} + \alpha^{r}$, $\alpha = a/(RT)$
B	second virial coefficient
β	isobaric expansion coefficient
C	third virial coefficient
c	specific heat capacity
δ	reduced density, ρ/ρ_c
f	fugacity
g	specific Gibbs free energy
h	specific enthalpy
N	number of data
μ	Joule-Thomson coefficient
κ	isothermal compressibility
p	pressure
R	gas constant
ρ	mass density
s	specific entropy
T	temperature
τ	inverse reduced temperature, T_c/T
u	specific internal energy
v	specific volume
w	speed of sound
Z	compressibility factor

Subscripts

p	process at constant pressure
v	process at constant volume
c	critical parameters
s	saturation

Superscripts

$'$	saturated-liquid state
$''$	saturated-vapor state
r	residual part
o	ideal-gas part
out	rejected

REFERENCES

1. R. Tillner-Roth, *Int. J. Thermophys.* **16**:91 (1995).
2. R. Span and W. Wagner, *Int. J. Thermophys.* **24**:111 (2003).
3. S. L. Outcalt and M.O. McLinden, *J. Phys. Chem. Ref. Data* **25**:605 (1996).

4. T. Tamatsu, H. Sato, and K. Watanabe, *Int. J. Refrig*. **16**:347 (1993).
5. I M. Astina and H. Sato, *Int. J. Thermophys*. **24**:963 (2003).
6. I M. Astina and H. Sato, *Int. J. Thermophys*. **25**:113 (2004).
7. I M. Astina and H. Sato, *Fluid Phase Equilib*. **221**:103 (2004).
8. Y. Higashi, M. Ashizawa, Y. Kabata, T. Majima, M. Uematsu, and K. Watanabe, *JSME Int. J*. **30**:1106 (1987).
9. A. Mizuoka, M.S. Thesis, Keio University (2001).
10. J. W. Magee, *Int. J. Thermophys*. **19**:1397 (1998).
11. J. P. Mohr and B. N. Taylor, *J. Phys. Chem. Ref. Data* **28**:1713 (1999).
12. V. Z. Geller, E. G. Porichanskii, P. I. Svetlichnyi, and Y. G. Elkin, *Kholod. Tekh. Tekhnol*. **29**:43 (1979).
13. R. Tillner-Roth and H. D. Baehr, *J. Chem. Thermodyn*. **25**:277 (1993).
14. M. Dressner and K. Bier, *Fortschr.-Ber. VDI*, **3**:332 (1993).
15. R. Tillner-Roth and H. D. Baehr, *J. Chem. Thermodyn*. **24**:413 (1992).
16. W. Blanke and R. Weiss, *Fluid Phase Equilib*. **80**:179 (1992).
17. J. W. Magee, *Int. J. Thermophys*. **19**:1381 (1998).
18. T. Hozumi, T. Koga, H. Sato, and K. Watanabe, *Int. J. Thermophys*. **14**:739 (1993).
19. K. A. Gillis, *Int. J. Thermophys*. **18**:73 (1997).
20. O. V. Beliajeva, A. Z. Grebenkov, T. A. Zayats, and B. D. Timofejev, *Dokl. Akad. Nauk SSSR* **38** (1994).
21. A. J. Grebenkov, O. V. Beliajeva, T. A. Zajatz, and B. D. Timofejev, in *Proc. 4th Asian Thermophys. Props. Conf*. (Tokyo, 1995), p. 311.
22. A. Yokozeki, H. Sato, and K. Watanabe, *Int. J. Thermophys*. **19**:89 (1998).
23. C. D. Holcomb, V. G. Niesen, L. J. Van Poolen, and S. L. Outcalt, *Fluid Phase Equilib*. **91**:145 (1993).
24. Y. Kabata, Y. Higashi, M. Uematsu, and K. Watanabe, *Trans. JAR* **5**:97 (1988).
25. A. Kamei, C. C. Piao, H. Sato, and K. Watanabe, *ASHRAE Trans*. **96**:141 (1990).
26. M. O. McLinden, *Scientific Assessment of Stratospheric Ozone*, Vol. II, Global Ozone Research and Monitoring Project, Report No. 20 (1989).
27. W. H. Mears, R. F. Stahl, S. R. Orfeo, R. C. Shair, L. F. Kells, W. Thompson, and H. McCann, *Ind. Eng. Chem*. **47**:1449 (1955).
28. J. Wang, Z. G. Liu, L. C. Tan, and J. M. Yin, *Fluid Phase Equilib*. **80**:203 (1992).
29. H. D. Baehr and R. Tillner-Roth, *J. Chem. Thermodyn*. **23**:1063 (1991).
30. H. A. Duarte-Garza and J. W. Magee, *Int. J. Thermophys*. **20**:1467 (1999).
31. E. Fransson, A. Barreau, and J. Vidal, *J. Chem. Eng. Data* **37**:521 (1992).
32. H. Sato, M. Uematsu, K. Watanabe, and M. Okada, *Fluid Phase Equilib*. **36**:167 (1987).
33. A. M. Silva and L. A. Weber, *J. Chem. Eng. Data* **38**:644 (1993).
34. R. Tillner-Roth, *Int. J. Thermophys*. **17**:1365 (1996).
35. N. Yada, M. Uematsu, and K. Watanabe, *Trans. JAR* **5**:107 (1988).
36. Z. Y. Zhao, J. M. Yin, and L. C. Tan, *Fluid Phase Equilib*. **80**:191 (1992).
37. D. R. Defibaugh and M. R. Moldover, *J. Chem. Eng. Data* **42**:160 (1997).
38. A. Iso and M. Uematsu, *Physica A* **156**:454 (1989).
39. K. H. U. Strom and U. B. Gren, *J. Chem. Eng. Data* **38**:18 (1993).
40. O. V. Beliajeva, A. J. Grebenkov, T. A. Zajatz, and Timofejev, *Int. J. Thermophys*. **20**:1689 (1999).
41. M. G. He, Z. G. Liu, and J. M. Yin, *Int. J. Thermophys*. **23**:1599 (2002).
42. D. A. Gunther and F. Steimle, *Int. J. Refrig*. **20**:235 (1997).
43. H. Kubota, *Chemistry Express* **2**:397 (1987).
44. S. Nakagawa, T. Hori, H. Sato, and K. Watanabe, *J. Chem. Eng. Data* **38**:70 (1993).

45. E. G. Porichanski, O. P. Ponomareva, and P. I. Svetlichny, *Izv. Vyssh. Uchebn. Zaved. Energ*. **3**:122 (1982).
46. H. Sato and K. Watanabe, *High Temp. High Press*. **26**:691 (1994).
47. J. Otto and W. Thomas, *Int. J. Heat Mass Transfer* **1**:41 (1964).
48. H. Sato, T. Kojima, and K. Ogawa, *Int. J. Thermophys*. **23**:787 (2002).